Sensors & Transducers, Vol. 156, Issue 9, September 2013, pp. 310-316

www.sensorsportal.com

Sensors & Transducers

http://www.sensorsportal.com

Synthesis, Characteristics and Enhanced Sulfur Dioxide Sensing Properties of Cu-doped SnO_2 Microspheres

*** Shudi Peng, Gaolin Wu, Wei Song**

Chongqing Electric Power Research Institute, Chongqing, 401123, China

* Tel.: +86-23-63230512, fax: +86-23-63230512

E-mail: pengshudi@163.com, 13983842134@139.com, 48012641@qq.com

Received: 5 August 2013 /Accepted: 25 August 2013 /Published: 30 September 2013

Abstract: Sulfur dioxide (SO_2) is a typical sulfur hexafluoride (SF_6) decomposition by product in gas insulated switchgear (GIS). Online monitoring and analyzing SO_2 gas concentration can timely and effectively evaluate the insulation performance of SF_6-gas-insulated apparatus. In this study, pure and 3 at % Cu-doped SnO_2 microspheres were synthesized via a simple and facile hydrothermal method, and were characterized by X-ray powder diffraction, field emission scanning electron microscopy, transmission electron microscopy, energy dispersive X-ray spectroscopy and X-ray photoelectron spectroscopy, respectively. Chemical gas sensors were fabricated with the conventional indirect heating technology and their gas sensing properties versus SO_2 were investigated in detail. The gas sensor fabricated with 3 at % Cu-doped SnO_2 microspheres exhibits lower optimum operating temperature and higher gas response than that of pure SnO_2 microspheres. Meanwhile, it demonstrates good stability and fast response-recovery. Most importantly, this sensor holds excellent discrimination with other SF_6 decompositions, including SOF_4, SOF_2, SO_2F_2 and HF. All results provide a good candidate in fabricating high-performance SO_2 sensor in practice. *Copyright © 2013 IFSA.*

Keywords: Sulfur dioxide, Gas sensing properties, Cu-doped SnO_2, Chemical gas sensor.

1. Introduction

Gas insulated switchgear (GIS) filled with pressurized SF_6 gas for electrical insulation and arc extinction, has been widely used in electrical power systems in the past decades [1-3]. When compared with the conventional open high-voltage switchgear installations, GIS has the advantages of small floor space, high stability and reliability, high-strength insulation, lower maintenance cost, and so on [4-5]. Despite these excellent advantages, there still exist some unavoidable insulation defects in GIS design, preparation, installation and running process. Partial discharge (PD) may occur at these insulation defects and cause SF_6 gas decomposition [6-7].

Till now, researches both at home and aboard have reported that SOF_4, SOF_2, SO_2F_2, SO_2 and HF are the mainly characteristic decompositions of SF_6 gas in GIS apparatus [8-10]. So it is available and effective to evaluate the insulation performance of SF_6 in GIS through detecting and analyzing these decomposed chemical products [11-12].

In recent years, interest in SF_6 decompositions detection has been greatly stimulated, and numerous methods have been reported, such as semiconductor gas sensors [1, 8, 10], spectroscopy [9] and carbon nanotubes [11, 12]. Peng *et al.* [1] successfully synthesized flower-like ZnO nanorods and investigated their gas sensing properties to SOF_2, SO_2F_2, and SO_2. Zhang *et al.* [11] reported the adsorption properties of SF_6 decomposition products adsorbed on single-walled carbon nanotubes (SWNT) from the first principles calculation. However, some limitations still need to be further improved

Article number P_1362

[1, 8, 10, 11], such as high operating temperature, low gas response and especially poor selectivity with potential interference gases.

Hence, in this study, we reported a simple and facile hydrothermal method to prepare pure and Cu-doped SnO_2 microspheres. Gas sensors were fabricated with traditional indirect heating technology and gas sensing properties of the fabricated sensors to SO_2 gas were measured in detail, including optimum operating temperature, gas response, response and recovery time, stability and reproducibility. Moreover, cross sensitivity and selectivity between SO_2 gas and other SF_6 decompositions were also investigated. Finally, a possible sensitivity mechanism was proposed.

2. Experimental

2.1. Synthesis of Materials

All chemicals were analytical-grade reagents purchased from Chongqing Chuandong Chemical Reagent Co. Ltd. and were used as received without any further purification. In this study pure and 3 at % Cu-doped SnO_2 microspheres were synthesized with a simple and facile hydrothermal method. The detailed synthesis processes were as follows:

In a typical synthesis process of 3 at % Cu-doped SnO_2 microspheres [13-15]: 2.104 g (6.0 mmol) of $SnCl_4 \cdot 5H_2O$, 0.031 g (0.18 mmol) of $CuCl_2$, and 1.080 g of NaOH were dissolved completely into 30 ml distilled water and 30 ml absolute ethanol in a beaker of 100 ml capacity. Then 0.588 g (2.0 mmol) of $C_6H_5Na_3O_7 \cdot 2H_2O$ (≥99.5 %) and 2.5 ml EG were added to the beaker. The mixture was magnetically stirred for 30 min to generate a transparent solution and then transferred into a 100 ml Teflon-lined stainless steel autoclave, sealed and maintained at 160 °C for 18 h in an electric furnace. After the heating treatment, the autoclave was cooled to room temperature naturally. Finally the products were harvested by centrifugation, washed three times with distilled water and absolute ethanol, respectively, and dried at 100 °C overnight to remove the solvent.

Pure SnO_2 microspheres were obtained in a similar process as 3 at % Cu-doped SnO_2 microspheres, but no addition of copper salt $CuCl_2$ was added to the precursor mixture.

2.2. Structure Characterization

The crystalline structures of the as-prepared pure and 3 at % Cu-doped SnO_2 microspheres were investigated by X-ray powder diffraction (XRD, Rigaku D/Max-1200X) with Cu Kα radiation, 40 kV, 200 mA, λ=1.5418 Å, and 2θ ranging from 20° to 80°. The surface morphologies of the samples were characterized with a Nova 400 Nano field emission scanning electron microscope (FESEM, Hillsboro equipped with energy dispersive X-ray (EDX) spectroscopy) and transmission electron micrographs (TEM, Hitachi S-570). Analysis of the X-ray photoelectron spectra (XPS) was performed on an ESCLAB MKII using Al as the exciting source.

2.3. Fabrication of Gas Sensor

Chemical gas sensors were fabricated with the conventional indirect heating technology [14]. Each obtained sample was ground into fine powder and mixed with absolute ethanol and deionized water in a weight ratio of 8:1:1 to form a homogenous paste. Then the paste was coated on an alumina ceramic tube to form a sensing film with a thickness of about 350 μm, where a pair of Au electrodes was previously printed. Pt lead wires were attached to the as-printed Au electrodes to collect the electrical signals.

After the ceramic tube was calcined at 300 °C in an electric furnace for 2 h, a Ni–Cr heating wire was inserted into the alumina tube as a heater controlling the operating temperature of sensing material as shown in Fig. 1. The tube was welded on the sensor pedestal. The distance between the two Au electrodes is estimated to be 6 mm and the diameter of the alumina tube is 1.2 mm. Finally, the sensor was further aged in an aging chamber at 120 °C for 36 h to improve the stability and repeatability. Fig. 2 is the photography of as-fabricated chemical gas sensor.

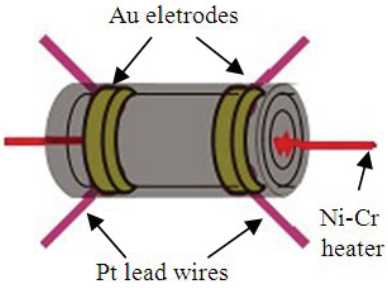

Fig. 1. Structure representation of the ceramic tube.

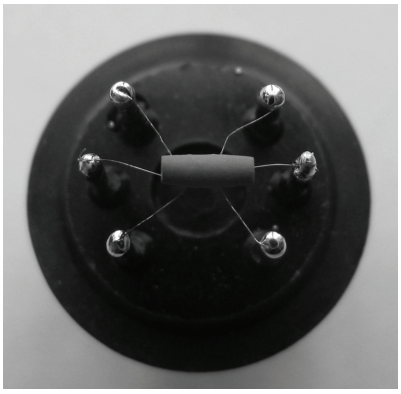

Fig. 2. A photography of the fabricated indirect heating gas sensor.

2.4. Gas Sensing Property Measurement

Gas sensing properties of the as-fabricated sensors were measured by a CGS-8 [14] (Chemical gas sensor-8) intelligent gas sensing analysis system purchased from Beijing Elite Tech Co., Ltd, China, as shown in Fig. 3. The sensors were pre-heated at different operating temperatures for about 30 min. When the resistances of all the sensors were stable, saturated target gas was injected into the test chamber (20 l in volume) by a microinjector through a rubber plug. The saturated target gas was mixed with air by two fans in the analysis system.

After the sensor resistances reached a new constant value, the test chamber was opened to recover the sensors in air. The sensor resistance, gas response, ambient temperature and humidity values were recorded timely and automatically by the intelligent gas sensing analysis system.

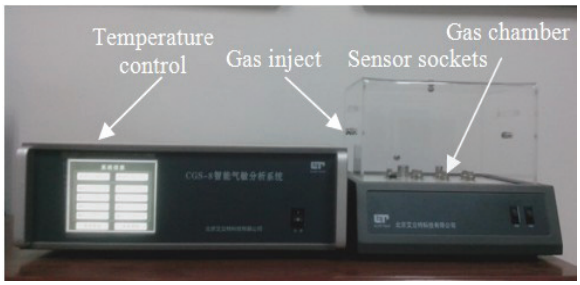

Fig. 3. Schematic image of the CGS-8 intelligent gas sensing measuring equipment.

The gas response value S was defined as S=Ra/Rg, where Ra was the sensor resistance value in air and Rg was that in a mixture of target gas and air [15]. The time taken by the sensor to reach 90 % of the total resistance change was defined as the response time in the case of gas adsorption or the recovery time in the case of gas desorption [13]. All measurements were repeated several times to ensure the repeatability and stability of the sensor.

3. Results and Discussion

3.1. Structural Characterization

XRD measurement was first performed to characterize the crystalline structure and chemical composition of the as-synthesized products. As shown in Fig. 4 all the diffraction peaks of pure and Cu-doped SnO_2 microspheres were well indexed to the standard data file of rutile SnO_2 (JCPDS file no. 41-1445, space group $P4_2/mnm$). No diffraction peaks from any impurities were detected, which means a high purity of our prepared samples. And there are no characteristic peaks from dopants, which may be attributed to the high dispersion or the poor crystallinity of copper related nanostructures.

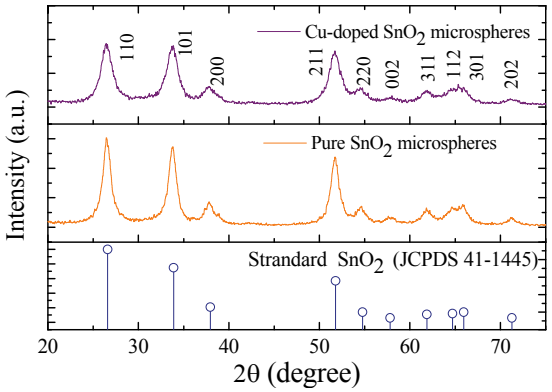

Fig. 4. XRD patterns of the prepared SnO_2 microspheres.

To check whether dopants have been successfully doped into the synthesized nanostructures, EDS analysis was conducted. As shown in Fig. 5 characteristic energy spectrum of Cu element appeared at 0.98, 8.09 and 8.87 keV, which confirms the availability of dopants Cu on the SnO_2 matrix. The composition of the Cu dopant is calculated to be about 2.92 at %, which matches well with its nominal concentration.

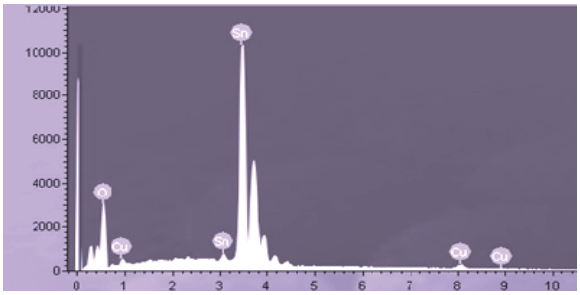

Fig. 5. EDS spectra of 3 at % Cu-doped SnO_2 microspheres.

XPS data of the 3 at % Cu-doped SnO_2 microspheres is collected and presented in Fig. 6 to further confirm the existence of Cu element and their valences. Fig. 6 (a) shows its wide spectrum, which is mainly consisted of Sn, O and Cu elements. The binding energies in Fig. 6 (b) at 486.5 and 493.8 eV correspond to Sn^{4+} of rutile SnO_2. From the narrow spectrum of Cu element as shown in Fig. 6 (c), the peak at 934.23 eV is identified as Cu $2p_{3/2}$, which possibly can be attributed to Cu^{2+} ions (933.90 eV). And it ruled out the presence of metallic Cu and CuO_2 in our sample, whose binding energy is 932.60 eV and 932.90 eV in standard XPS data, respectively.

Thus, based on the XRD, EDS and XPS results, the Cu^{2+} ions are believed to be successfully incorporated into the SnO_2 nanocrystals.

FESEM were further used to investigate the surface morphologies and microstructures of the synthesized samples. Fig. 7 (a) and Fig. 7 (b) illustrate the FESEM images of pure and 3 at % Cu-doped SnO_2 nanostructures, respectively.

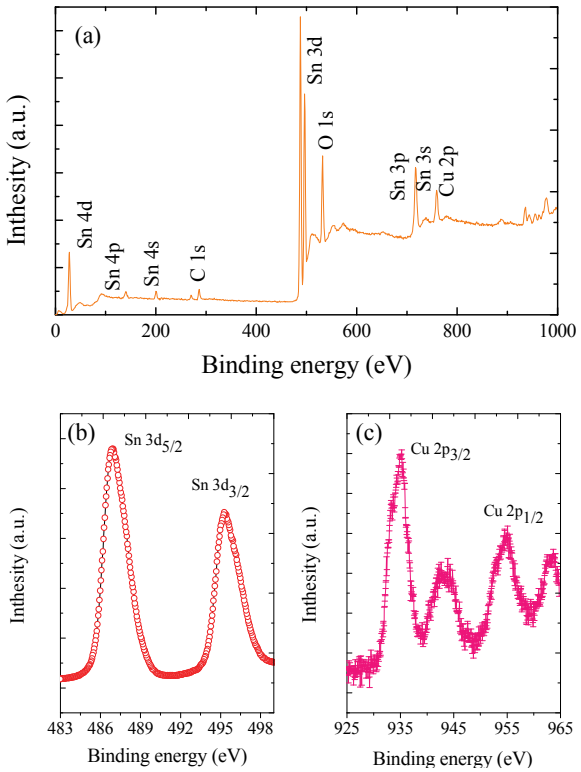

Fig. 6. XPS spectra of 3 at % Cu-doped SnO_2 microspheres (a) wide spectrum (b) Sn 3d and (c) Co 2p.

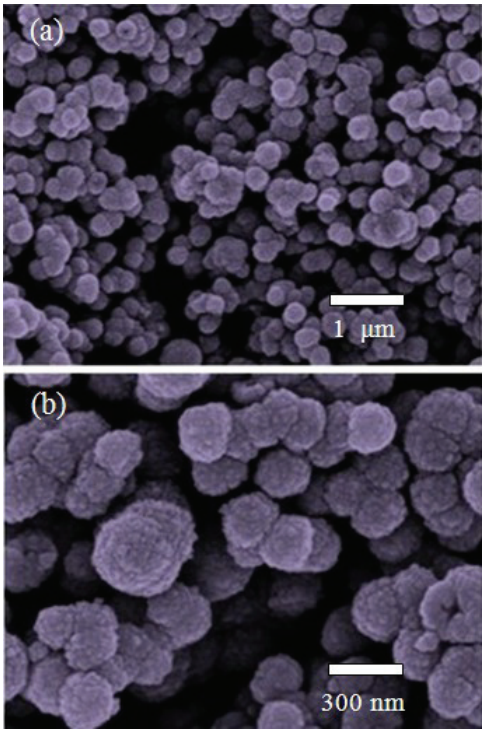

Fig. 7. FESEM images of (a) pure and (b) 3 at % Cu-doped SnO_2 microspheres.

One can clearly see in Fig. 7 that both samples are made up of a large scale of SnO_2 microspheres. These spheres are uniform in size and shape with good dispersion in the whole FESEM images. Cu doping in our experiments has nearly no influence on the morphology of SnO_2 nanostructures. The diameters of both samples are in the scope of 200 to 250 nm.

Fig. 8 shows typical TEM and HRTEM images of 3 at % Cu-doped SnO_2 nanostructures. As shown in Fig. 8 (a) that the single microsphere is composed of many SnO_2 particles with average diameter of 2-3 nm. Fig. 8 (b) shows a HRTEM image of 3 at % Cu-doped SnO_2 sample, and the fringe space is measured to be about 0.335 nm, which is consistent well with the (110) plane of rutile SnO_2.

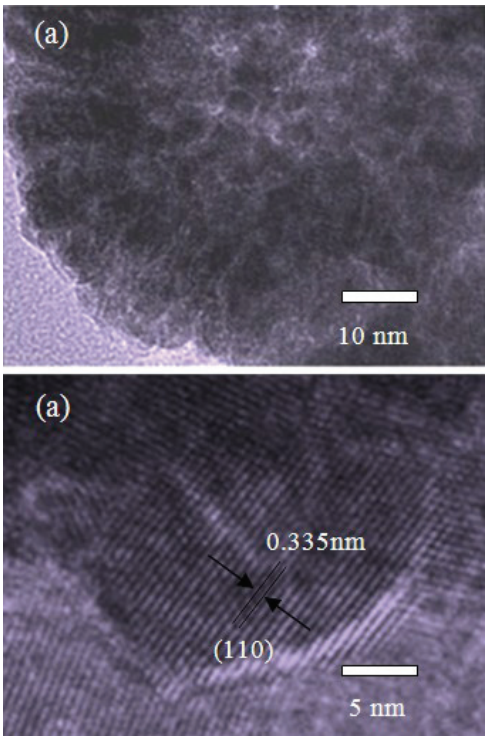

Fig. 8. TEM and HRTEM images of 3 at % Cu-doped SnO_2 microspheres.

3.2. Gas Sensing Properties

Gas sensing properties of the as-fabricated sensors are investigated in detail as follows.

The gas responses of the pure and Cu-doped SnO_2 based sensors to 30 ppm of SO_2 with working temperature from 150 to 450 °C were firstly measured and shown in Fig. 9. One can see that the 3 at % Cu-doped sensor exhibits exclusive lower operating temperature than that of pure sensor. It is measured to be about 300 °C and 275 °C for pure and 3 at % Cu-doped sensors. And the highest gas response of the pure and 3 at % Cu-doped sensors versus 30 ppm of SO_2 is estimated to be about 43.15 and 23.37 respectively.

Fig. 10 shows the gas responses of the 3 at % Cu-doped sensor towards SO_2 at 275 °C with gas concentration from 1 to 500 ppm. One can clearly see in Fig. 10 that the gas response of the sensor increases rapidly with increasing SO_2 concentration

below 50 ppm. And then the sensor shows a slower increase with further increasing the gas concentration from 50 to 300 ppm, and finally reaches saturation at nearly about 500 ppm.

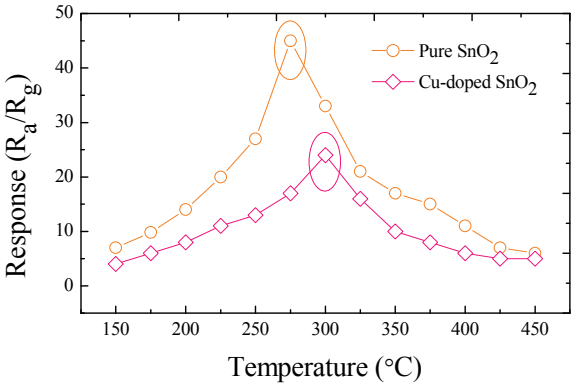

Fig. 9. Gas Response of the sensors to different operating temperature under 30 ppm of SO_2.

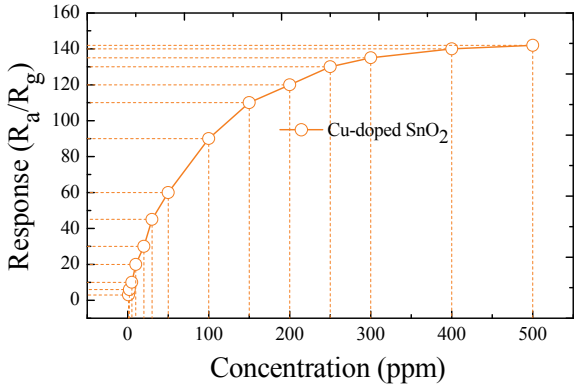

Fig. 10. Gas Response of the sensor versus SO_2 concentration from 1 to 500 pmm.

If the response of gas sensor matches linear or quasi-linear relationship with the concentration of target gas, the sensor can be applied to engineering application in practice. The linear fitting curve of the 3 at % Cu-doped sensor towards SO_2 at 275 °C with gas concentration from 1 to 50 ppm is shown in Fig. 11. As seen in Fig. 11 the linear correlation coefficient R^2 is estimated to be about 0.9869. Such a higher linear dependence implies the product a promising SO_2 sensing material.

Respons-recovery property and stability are other two key parameters to evaluate the sensing performances of semiconductor gas sensors. As shown in Fig. 12 the response and recovery time of the 3 at % Cu-doped sensor to SO_2 gas is measured to be about 5-8 s and 12-20 s, respectively. During the four testing cycles, the electric resistance of the sensor invariably returns to its initial value, which means good reproducibility and excellent stability of the as-prepared sensor for SO_2 detection.

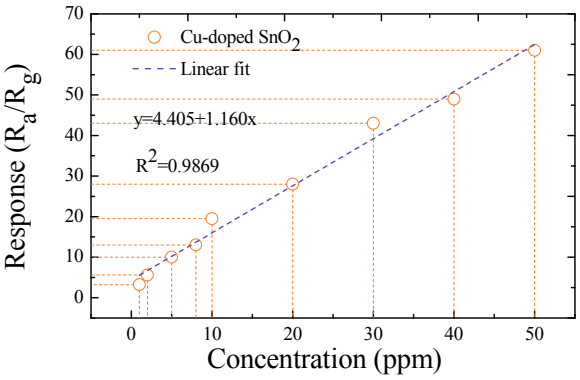

Fig. 11. Gas Response of the sensor versus SO_2 concentration from 1 to 50 pmm.

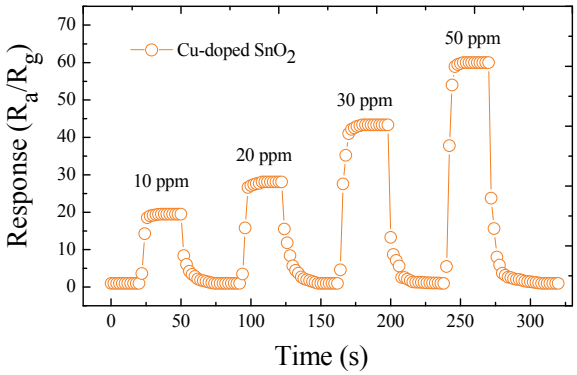

Fig. 12. Response and recovery characteristics of the sensor to 10, 20, 30 and 50 ppm of SO_2.

Selectivity is another very important indicator for semiconductor sensors, especially with potential interference gases. Fig. 13 depicts the gas response histogram of the 3 at % Cu-doped sensor exposed to 10 and 30 ppm of SO_2 and other SF_6 decomposition byproducts, including SOF_4, SOF_2, SO_2F_2, and HF. The results imply that the sensor is sensitive to SO_2, but nearly insensitive to SOF_4, SOF_2, SO_2F_2 and HF. Thus, the 3 at % Cu-doped sensor exhibits high selectivity to SO_2 with other SF_6 decompositions.

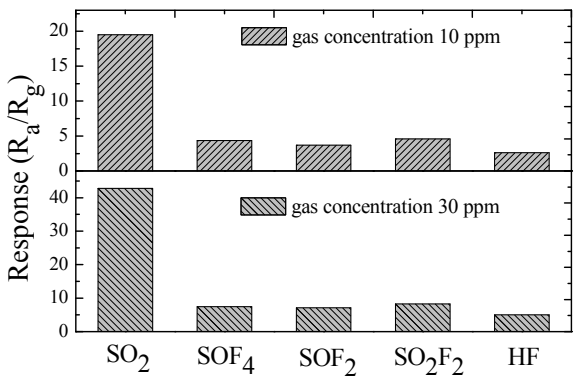

Fig. 13. Selectivity of the sensor to 10 and 30 ppm of SO_2, SOF_4, SOF_2, SO_2F_2 and HF.

The sensing process of SO_2 adsorbed on SnO_2 based sensors has discussed in our former paper [1]. A possible sensing mechanism for the enhanced SO_2 sensing properties was discussed as follows. The enhanced SO_2 sensing performances of the present Cu-doped SnO_2 microspheres may be attributed to two main aspects. The first one is relating to the possible chemical effect of the catalytic activity of CuO nanoparticles. CuO is a far better oxygen dissociation catalyst than SnO_2 [16], adsorbed oxygen can diffuse faster to surface vacancies and capture electrons from the conduction band of SnO_2 to generate various kinds of chemical adsorbed oxygen species, namely O_2^-, O^{2-} and O^- [1, 17]. The second aspect can be attributed to the synergic interaction between CuO nanoparticles and SnO_2 microspheres. An additional barrier and depletion layer at the interface of CuO-SnO_2 may be formed, accelerating the charge transfer between valence band and conduction band in the sensing process [18]. Thus, an excellent SO_2 sensing property are observed in our measurements.

4. Conclusions

In conclusion, pure and 3 at % Cu-doped SnO_2 microspheres were successfully synthesized via a simple and facile hydrothermal method and characterized by XRD, EDS, XPS, SEM and TEM. Chemical gas sensors were fabricated with the conventional indirect heating technology and sensors properties were investigated in detail. The optimum operating temperature of the pure and Cu-doped sensor versus SO_2 is measured to be above 275 °C and 300 °C. The Cu-doped one exhibits high-linear gas response with R^2=0.9869 to 1-50 ppm SO_2 and its response and recovery time is measured to be about are 5-8 s and 12-20 s. Moreover, the 3 at % Cu-doped SnO_2 sensor shows a remarkable discrimination between SO_2 and other SF_6 decomposition byproducts. Therefore, the 3 at % Cu-doped SnO_2 microspheres may be potentially exploited into an effective SO_2 sensing material for chemical sensors.

References

[1]. S. D. Peng, G. L. Wu, W. Song, Q. Wang, Application of flower-like ZnO nanorods gas sensor for detecting SF6 decompositions, *Journal of Nanomaterials*, Vol. 2013, Issue 1, 2013, pp.1-9.

[2]. J. Tang, F. Liu, X. X. Zhang, Q. H. Meng, J. B. Zhou, Partial discharge recognition through an analysis of SF6 decomposition products part 1: decomposition characteristics of SF6 under four different partial discharges, *IEEE Transactions on Dielectrics and Electrical Insulation*, Vol. 19, Issue 1, 2012, pp. 29-36.

[3]. J. Tang, F. Liu, X. X. Zhang, Q. H. Meng, J. G. Tao, Partial discharge recognition through an analysis of SF6 decomposition products part 2: feature extraction and decision tree-based pattern recognition, *IEEE Transactions on Dielectrics and Electrical Insulation*, Vol. 19, Issue 1, 2012, pp. 37-44.

[4]. I. Sauers, H. W. Ellis, L. G. Christophoro, Neutral decomposition products in spark breakdown of SF6, *IEEE Transactions on Electrical Insulation*, Vol. 21, Issue 2, 1986, pp. 111-120.

[5]. R. J. Van Brunt, J. T. Herron, Fundamental processes of SF6 decomposition and oxidation in glow and corona discharges, *IEEE Transactions on Electrical Insulation*, Vol. 25, Issue 1, 1990, pp. 75-94.

[6]. M. L. Shih, W. J. Lee, C. H. Tsai, P. J. Tsai, C. Y. Chen, Decomposition of SF6 in an RF plasma environment, *Journal of the Air & Waste Management Association*, Vol. 52, Issue 11, 2002, pp. 1274-1280.

[7]. W. T. Tsai, The decomposition products of sulfur hexafluoride (SF6): reviews of environmental and health risk analysis, *Journal of Fluorine Chemistry*, Vol. 128, Issue 11, 2007, pp. 1345-1352.

[8]. J. Singh, A. Mukherjee, S. K. Sengupta, J. Im, G. W. Peterson, Sulfur dioxide and nitrogen dioxide adsorption on zinc oxide and zirconium hydroxide nanoparticles and the effect on photoluminescence, *Applied Surface Science*, Vol. 258, Issue 15, 2012, pp. 5778-5785.

[9]. R. Kurte, C. Beyer, H. M. Heise, D. Klockow, Application of infrared spectroscopy to monitoring gas insulated high-voltage equipment: electrode material-dependent SF6 decomposition, *Analytical and Bioanalytical Chemistry*, Vol. 373, Issue 7, 2002, pp. 639-646.

[10]. X. X. Zhang, J. B. Zhang, Y. C. Jia, P. Xiao, J. Tang, TiO2 nanotube array sensor for detecting the SF6 decomposition product SO_2, *Sensors*, Vol. 12, Issue 3, 2012, pp. 3302-3313.

[11]. X. X. Zhang, J. B. Zhang, J. Tang, B. Yang, Gas-sensing simulation of single-walled carbon nanotubes applied to detect gas decomposition products of SF6, *Journal of Computational and Theoretical Nanoscience*, Vol. 9, Issue 8, 2012, pp. 1096-1100.

[12]. W. D. Ding, R. Hayashi, K. Ochi, J. Suehiro, K. Imasaka, Analysis of PD-generated SF6 decomposition gases adsorbed on carbon nanotubes, *IEEE Transactions on Dielectrics and Electrical Insulation*, Vol. 13, Issue 6, 2006, pp. 1200-1207.

[13]. W. G. Chen, Q. Zhou, X. P. Su, L. N. Xu, S. D. Peng, Morphology control of tin oxide nanostructures and sensing performances for acetylene detection, *Sensors & Transducers*, Vol. 154, Issue 7, July 2013, pp. 195-200.

[14]. Q. Zhou, W. G. Chen, L. N. Xu, S. D. Peng, Study on sensing properties and mechanism of Pd-doped SnO_2 sensor for hydrogen and carbon monoxide, *Sensors & Transducers*, Vol. 151, Issue 4, 2013, pp. 84-89.

[15]. L. L. Wang, Z. Lou, T. Zhang, H. T. Fan, X. J. Xu, Facile synthesis of hierarchical SnO_2 semiconductor microspheres for gas sensor application, *Sensors and Actuators B-Chemical*, Vol. 155, Issue 1, 2011, pp. 285-289.

[16]. H. X. Gao, Y. Luo, H. X. Hao, Y. Gao, H. Wang, S. W. Li, CuO-SnO_2 nanocomposite powders: synthesis and characterization, *Chinese Journal of Inorganic Chemistry*, Vol. 21, Issue 8, 2005, pp. 1218-1222.

[17]. W. Wei, Y. Dai, B. B. Huang, Role of Cu doping in SnO_2 sensing properties toward H_2S, *Journal of*

Physical Chemistry C, Vol. 115, Issue 38, 2011, pp. 18597-18602.
[18]. L. Liu, T. Zhang, L. Y. Wang, S.C. Li, Improved ethanol sensing properties of Cu-doped SnO_2 nanofibers, *Materials Letters*, Vol. 63, Issue 23, 2009, pp. 2041-2043.